Fabrication of ice-templated macroporous TiO_2–chitosan scaffolds for photocatalytic applications†

Cheewita Suwanchawalit,[a] Avinash J. Patil,*[b] Ravinash Krishna Kumar,[b] Sumpun Wongnawa[a] and Stephen Mann*[b]

Received 29th June 2009, Accepted 28th August 2009
First published as an Advance Article on the web 12th October 2009
DOI: 10.1039/b912698h

Higher-ordered 3D macroporous TiO_2-functionalized chitosan scaffolds were prepared by ice segregation induced self-assembly (ISISA), in which homogenous dispersions of 6, 27 or 200 nm sized TiO_2 nanoparticles and chitosan cross-linked with glycidoxypropyltrimethoxysilane were unidirectionally frozen at −196 °C. Scanning electron microscopy showed that under established optimum conditions the monoliths comprised well-aligned 30–50 μm sized micro-channels running parallel to the direction of ice growth. The surface morphology of the internal wall structure was influenced by the size of the titania nanoparticles. Scaffolds prepared in the presence of 6 nm sized anatase particles showed featureless walls with concealed/embedded nanoparticles, whereas larger TiO_2 particles remained exposed at the surface of the channel walls. Mechanical properties of the composite scaffolds were studied under compressive loads and stress–strain measurements obtained, and the effect of particle size on the elastic properties of the macroporous constructs determined. The hybrid scaffolds were shown to be reusable substrates for the photocatalytic degradation of methylene blue and Orange II dye molecules.

Introduction

Architectural constructs of multifunctional organic/inorganic composite materials play a central role in the burgeoning field of organized materials chemistry.[1] Of particular interest are hybrid materials in the form of three-dimensional (3D) scaffolds that comprise functional components arranged within a hierarchical network of pores extending across multiple length scales. These materials can be prepared as colloidal crystals, powders, discrete micro-spheres, membranes, fibers or monoliths by employing sacrificial templates such as self-assembled surfactant or polymer micelles, biomolecules or organic/inorganic colloidal particles.[2,3] They have myriad potential applications such as catalytic supports, high-performance adsorbents, electrical insulators, photonic media and membranes for separation processes.[1–4] Among these, monoliths comprising interconnected hierarchical micro-/meso-/macroporous networks with large mass transfer properties are of particular interest as new materials in tissue engineering, automotive technology, separation processes and organic waste treatments. In such materials, the macropores promote mass transfer and minimize the pressure drop inside the monoliths, whilst the micro-/mesopores provide a large surface area that facilitates catalytic and adsorption processes.[5] Several methods, such as emulsion freeze-drying,[6] phase separation,[7] porogen leaching,[8,9] polymer foaming[10] and gel-templating,[11] have been used to fabricate porous monoliths comprising bimodal or even trimodal pore structures. However, these methods are often compromised by the judicious control required to remove the template such that intact monoliths with a higher-order pore structure are produced. In contrast, methods based on ice segregation induced self-assembly (ISISA) are facile, inexpensive and environmentally benign, and have proven to be an effective route to the fabrication of a range of organic–inorganic macroporous scaffolds with various shapes and sizes.[12,13] In this cryochemical process, inorganic nanoparticulate sols or aqueous suspensions of polymers are transferred into a mould, which is then unidirectionally frozen in liquid nitrogen at −196 °C. As a consequence, arrays of polygonal ice crystals growing parallel to the freezing direction induce segregation and entrapment of the solute phase within the inter-crystalline domain boundaries. Subsequent sublimation and thawing of the ice produce intact porous monoliths in which a hierarchical pore network is generated as a replica of the ice crystal network. By selecting an appropriate solute phase, a range of functional bio(organic)–inorganic porous materials with desired functionality can be produced. For example, high-surface area macroporous scaffolds have been prepared by using silica[5,14,15] or titania sols[16] and various inorganic/metal nanoparticles.[17–20] Similarly, macroporous polymer composites have been produced by ice crystal templating of graphitic materials such as carbon nanotubes or unilamellar graphene sheets dispersed in appropriate polymeric suspensions.[20–23] In the present study, we extended the ISISA process to generate TiO_2-impregnated chitosan scaffolds with photocatalytic activity. The macroporous monoliths are stabilized in aqueous media by cross-linking the polysaccharide matrix with glycidoxypropyltrimethoxysilane,

[a]*Department of Chemistry, Faculty of Science, Prince of Songkla University, Hat Yai, Songkhla, 90112, Thailand*
[b]*Centre for Organized Matter Chemistry, School of Chemistry, University of Bristol, Bristol, UK BS8 1TS. E-mail: s.mann@bristol.ac.uk; Avinash.patil@bristol.ac.uk*

† Electronic supplementary information (ESI) available: PXRD and TEM of nanoparticles; SEM images of monoliths; EDXA mapping; photocatalysis profiles. See DOI: 10.1039/b912698h

and exhibit differences in microstructure, mechanical properties and photochemical activity depending on the particle size and surface charge of the incorporated TiO_2 particles. In addition, the TiO_2–chitosan scaffolds can be readily exploited for repeated photocatalytic use. As photoactive sols[3,25] are often difficult to separate from the reaction media, reusable macroporous TiO_2–chitosan monoliths could be of potential use in achieving high throughput in applications such as the photocatalytic degradation of organic pollutants.

Experimental

TiO_2 materials

Three types of TiO_2 were used: an as-prepared anatase sol (mean particle size = 6 nm), a potassium-doped anatase (K-TiO_2; 200 nm sized aggregates, 30 nm primary particles), and an as-received commercial powder (Degussa P25, anatase–rutile mixture, 27 nm) (see ESI,† Fig. S1 and S2).

A stable sol of anatase nanoparticles was prepared by methods reported previously.[25] In brief, 15 mL titanium isopropoxide were added drop-wise to 185 mL of acidified distilled water containing 1.3 mL HNO_3 (pH $\approx$ 1). The resulting white precipitate was peptized at 85 °C for 12 h under vigorous stirring in an open conical flask until a final volume of 50 mL was obtained. The resulting colloid was stable for several weeks.

Potassium oxalate-doped TiO_2 powders were prepared by our previously reported method involving a base-catalyzed sol–gel process.[26] Typically, 20 mL of $TiCl_4$ were added slowly to 100 mL of distilled water followed by addition of 70 mL of 1.3 M potassium oxalate solution to produce a white precipitate, which was refluxed at 90 °C for 13 h under vigorous stirring. The above suspension was then treated with hexamethylenetetramine ($C_6H_{12}N_4$, Fluka) until the pH of the suspension was 7 and maintained at 90 °C for a further 13 h. The white precipitate was subsequently filtered and washed with distilled water to remove chloride ions, dried at 105 °C for a day, ground to fine powder, and then calcined at 400 °C for 3 h to give the product, K-TiO_2.

Preparation of cross-linked chitosan (CS) gels

All chemicals were of analytical grade and used without further purification. A 2.5 wt% chitosan solution was prepared using 0.2 M acetic acid. 20 mL of the acidified chitosan solution were then cross-linked by mixing with 1 mL of γ-glycidoxypropyltrimethoxysilane (GPTMS, Gelest-ABCR; chitosan : GPTMS = 20 : 1, v/v), which was then employed for the fabrication of the macroporous scaffolds.[27]

Preparation of macroporous cross-linked chitosan–TiO_2 scaffolds

In a typical experiment, 1 mL of an as-prepared chitosan gel cross-linked with GPTMS was mixed with 1 mL of an aqueous suspension of K-TiO_2, P-25 or TiO_2 sols (50 mg mL^{-1}), and homogenized using a vortex mixer. The resulting cross-linked chitosan–TiO_2 (CS–TiO_2) gels were transferred to a plastic syringe (diameter 8 mm, length 4 cm, volume 2 mL) and subsequently immersed in a liquid nitrogen bath at a constant freezing rate of 5.9 mm min^{-1}. The unidirectionally frozen cryogels were then freeze-dried overnight and removed from the syringe as intact monoliths. Optimal conditions for fabrication of macroporous and mechanically stable CS–TiO_2 hybrid scaffolds were determined at a constant syringe (mould) size by changing the chitosan : titania nanoparticle ratios (v/v; 1 : 0.5, 1 : 1, 1 : 2, 1 : 4 and 1 : 8) and immersion rates (2, 5.9 and 15 mm min^{-1}). Vertical and cross-sections of the scaffold were prepared by cutting monoliths with a sharp razor blade. The internal morphology was examined by scanning electron microscopy (SEM).

Photocatalytic activity of cross-linked chitosan–TiO_2 scaffolds

The photocatalytic activities of the CS–TiO_2 scaffolds (diameter 4 mm, length 4 cm) were tested by investigating decolorization of methylene blue and Orange II dye solutions at room temperature. For this, cross-linked chitosan or CS–TiO_2 scaffolds were cut into cylindrical pieces and placed in a Petri dish containing 20 mL of methylene blue solution or Orange II solution (2.5×10^{-5} M). In each experiment, the Petri dish was kept in the dark for 1 h prior to UV light illumination to achieve adsorption and desorption equilibria. Subsequently, solutions were irradiated using a UV lamp (λ = 365 nm, model UVLS-28, USA), and at given irradiation time intervals (every 1 h), 2 mL of the sample were collected and the residual concentration of dye molecules measured by monitoring the change in absorbance at 665 nm and 485 nm for methylene blue and Orange II, respectively. Calibration graphs for each dye were used to determine time-dependent changes in dye concentration in the irradiated solutions. Control experiments in the absence of light or chitosan scaffolds prepared without TiO_2 were also performed.

Kinetic studies on photocatalytic degradation were modeled using a modified Langmuir–Hinshelwood equation, where the reaction rate, r, is proportional to the surface coverage, θ, by:

$$r = -\frac{dC}{dt} = k_r\theta = \frac{k_r KC}{1 + KC} \quad (1)$$

(k_r is the reaction rate constant, K the adsorption coefficient of the reactant, and C the reactant concentration at any time, t). For small values of C, KC is negligible with respect to unity and eqn (1) describes first-order kinetics. The integration of eqn (1) within the limits of $C = C_0$ at the start of radiation ($t = 0$) yields eqn (2):

$$-\ln\left(\frac{C}{C_0}\right) = k_r Kt = k_{app}t \quad (2)$$

$$i.e., \quad \ln\left(\frac{C_0}{C}\right) = k_{app}t \quad (3)$$

where the apparent first-order rate constant, $k_{app} = k_r K$.

Mechanical properties

Compression measurements were carried out using an Instron 3343 1 kN machine fitted with a 1000 N load cell. Scaffolds were cut into cylindrical sections of 8 × 8 mm, and stress–strain measurements plotted at a compression rate of 0.05 mm s^{-1}.

Characterization. Powder X-ray diffraction patterns were obtained using a Bruker D8 Advanced X-ray diffractometer with Cu K_α source (λ = 1.5418 Å). TEM analysis of TiO_2 nanoparticles was performed by using a JEOL 1200 EX microscope operating at 120 kV. Surface features and internal microstructures of the CS–TiO_2 scaffolds were examined by SEM (JSM-5600 LV). FTIR spectroscopy analysis was carried out using a Perkin Elmer Spectrum One spectrophotometer fitted with spectrum analysis software. Decolorization of dye solutions was monitored by recording change of absorbance using a Perkin-Elmer Lambda-25 UV-Vis spectrophotometer.

Results and discussion

Fabrication of monolithic 3D chitosan (CS) monoliths with ordered macroporosity was readily achieved by ice-templating procedures. However, the non-cross-linked materials lost their structural integrity when exposed to water due to redissolution of chitosan, and as such were of limited application. In contrast, monoliths prepared from chitosan hydrogels cross-linked with γ-glycidoxypropyltrimethoxysilane (GPTMS) were more mechanically stable and insoluble in aqueous solutions. Cross-linking was achieved by an acid catalyzed amino-oxirane addition reaction between the amino groups on the chitosan polymer chains and GPTMS.[27] This process was accompanied by hydrolysis and condensation of the linked GPTMS silanol groups to produce a cross-linked silica-polymer network. SEM images of vertical sections of the dried monoliths showed a network of co-aligned channels, 30–50 μm in size, which were oriented parallel to the direction of freezing of the hydrogel (Fig. 1a). As a consequence, the polysaccharide chains were compacted irreversibly within the channel walls by lateral compression between adjacent ice crystals during growth to produce an ordered macroporous matrix (Fig. 1b).

Chitosan–TiO_2 (CS–TiO_2) scaffolds were prepared using an as-synthesized anatase sol, a potassium-doped anatase (K-TiO_2) powder or an as-received commercial anatase/rutile powder (Degussa P25) (Fig. 2). Optimum fabrication conditions were established using as-synthesized anatase particles (size = 6 nm) to prepare CS–TiO_2 monoliths under a range of conditions including changes in the nanoparticle loading, freezing or immersion rates. At a constant syringe size (8 mm diameter) and freezing rate (5.9 mm min^{-1}), changes in the CS : TiO_2 (v/v) ratio across the range 1 : 0.5, 1 : 1, 1 : 2, 1 : 4 and 1 : 8 resulted in marked differences in internal architecture. In each case, longitudinal and cross-sections were taken from the middle part of the scaffold and the structures studied by SEM. Significantly, monoliths prepared using ratios higher than 1 : 1 comprised irregular or highly distorted microstructures (ESI† Fig. S3). This was attributed to the deleterious effect of relatively high concentrations of the TiO_2 sol on lowering the effective CS concentration due to strong adsorption of the polysaccharide onto the nanoparticles.[17] Disordered structures were also observed for monoliths prepared at relatively fast freezing rates (15 mm min^{-1}) compared with materials prepared under immersion speeds of 2 or 5.9 mm min^{-1} (ESI,† Fig. S4). This was consistent with previous studies that showed that the temperature gradient strongly influences the structure (amorphous/crystalline), and extent of lateral and vertical growth of the polygonal ice crystals.[17,18]

Given the above observations, optimum conditions for the reproducible formation of well-ordered macroporous CS–TiO_2 scaffolds were established at a CS : TiO_2 ratio of 1 : 1 with use of a 8 mm diameter mould and freezing rate of 5.9 mm min^{-1}. Under these conditions, scaffolds with levels of internal organization somewhat greater than the native cross-linked CS monoliths could be prepared using each of the three different aqueous dispersions of TiO_2 nanoparticles. In each case, SEM micrographs of cross-sections and longitudinal sections showed ordered channels with dimensions of 20–50 μm co-aligned along

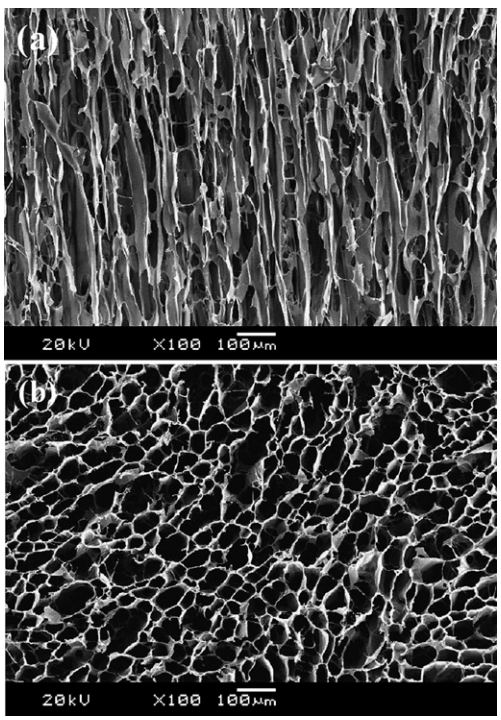

Fig. 1 SEM images of (a) longitudinal section (parallel to the freezing direction) of an organosilane cross-linked chitosan scaffold prepared by ice-templating and showing ordered capillaries and (b) cross-sectional view (perpendicular to ice growth) showing macroporous network.

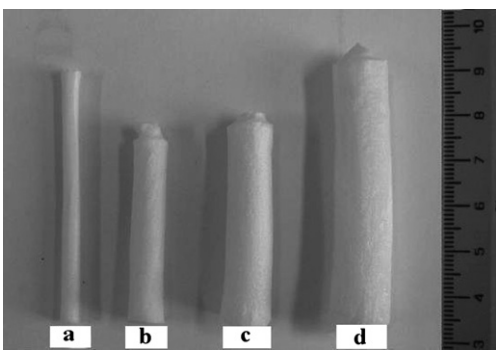

Fig. 2 Photographs of typical TiO_2–chitosan macroporous monoliths prepared with 6 nm sized TiO_2 (anatase) nanoparticles at a TiO_2 : chitosan ratio of 1 : 1 and immersion rate of 5.9 mm min^{-1} using syringe diameters of (a) 4 mm, (b) 8 mm, (c) 11 mm and (d) 13 mm.

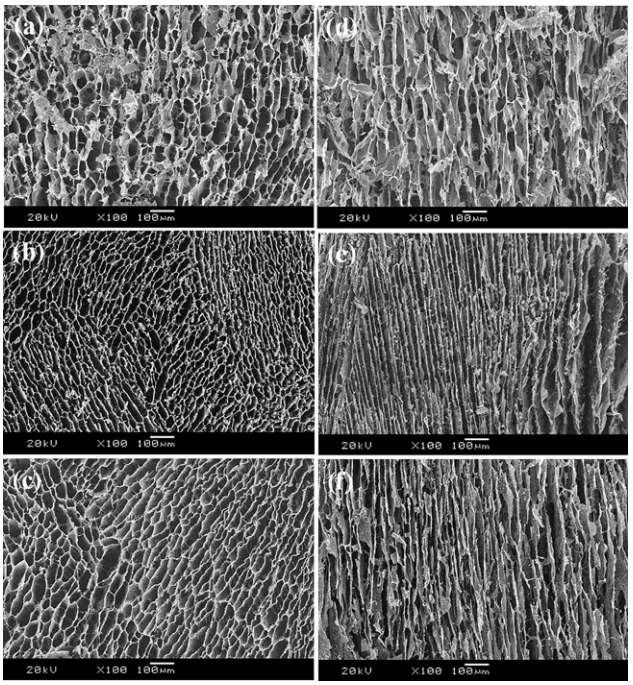

Fig. 3 SEM images showing internal microstructure of titania-functionalized chitosan scaffolds prepared with a TiO_2 : chitosan ratio of 1 : 1 and freezing rate of 5.9 mm min^{-1}. Cross-sectional views (left panels) and longitudinal sections (right panels) of macroporous monoliths prepared with (a,d) anatase nanoparticles, (b,e) P-25 titania and (c,f) K-TiO_2 anatase.

the direction of freezing (Fig. 3). In addition, high magnification SEM images revealed the presence of smooth, featureless channel walls for scaffolds prepared with anatase nanoparticles, suggesting that the 6 nm sized TiO_2 particles were encapsulated within the interior of the biopolymer matrix; in contrast, the channels and interconnected walls of CS–K-TiO_2 and CS–P25 monoliths were decorated with partially embedded particles that were exposed at the matrix surface (Fig. 4). EDX analysis and elemental mapping performed on various sections of the scaffolds confirmed the presence of Ti and Si, and showed a homogenous distribution of these elements throughout the monoliths (ESI† Fig. S5). This was consistent with FTIR spectra, which showed characteristic vibration frequencies corresponding to CH_2 (2869 cm^{-1}), OH (3423 cm^{-1}), N–H (1651 cm^{-1}) and Si–O–Si (1100 cm^{-1}) associated with the GPTMS-cross-linked CS matrix, as well as characteristic bands for Ti–O vibrations around 906 and 450 cm^{-1} (data not shown).[27,28]

Other experiments were undertaken to investigate the effect of incorporation of TiO_2 particles on the mechanical strength of the cross-linked chitosan scaffolds. For this, cylindrical sections (8 × 8 mm) were taken from regions proximal to the immersion end of the syringe (x) or middle zone (y) of the monoliths and subjected to load under compression. In each case, the stress–strain curves exhibited linear elasticity at low stress, which was then followed by a collapse plateau indicating buckling of the polymeric wall structure (Fig. 5). For each of three different types of TiO_2 colloid used, the average compressive moduli were slightly increased for the section taken from the middle zone (average values for x and y: control (0.05 and 0.13 MPa), anatase (0.41 and 0.63 MPa), K-TiO_2 (0.13 and 0.31 MPa) and P-25 (0.02 and 0.05 MPa)), which was consistent with the more ordered microstructure in this region of the monolith. Interestingly, monoliths comprising 6 nm sized anatase particles were significantly stronger than the other composites, and showed a well-defined elastic region, consistent with the embedding and immersion of these nanoparticles within the cross-linked polysaccharide matrix (see Fig. 4). Extensive integration of the nanoparticles presumably hinders buckling of the polymer chains to produce a stiffer composite when placed under compression. In contrast, the K-TiO_2-loaded scaffolds were significantly stiffer than unmineralized cross-linked chitosan, whilst the P-25-containing monoliths were brittle and often weaker than the polysaccharide matrix alone. These observations were attributed to the preferential location of these TiO_2 particles specifically on the walls of the internal microstructure.

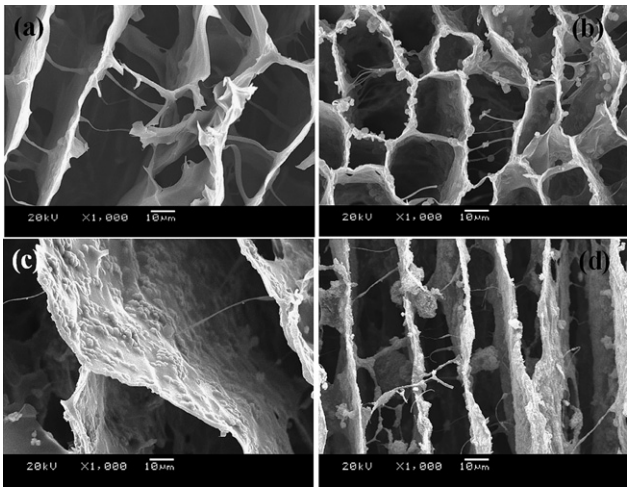

Fig. 4 High magnification SEM images showing effect of titania particle size on the morphology of the internal walls of CS–TiO_2 sponges. (a) Smooth walled microstructure produced in the presence of 6 nm sized anatase nanoparticles. (b,c) Roughened wall texture viewed at (b) low and (c) high magnification for scaffolds prepared with 200 nm sized K-TiO_2 nanoparticles. TiO_2 particles are clearly visible on the wall surface. (d) Similar morphological features as in (b,c) observed for P-25-containing CS scaffolds.

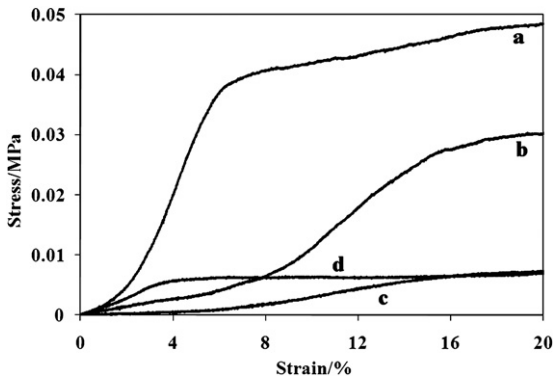

Fig. 5 Stress–strain curves for CS–TiO_2 scaffolds prepared using (a) TiO_2 anatase sol, (b) K-TiO_2 powders, (c) P-25 and (d) chitosan scaffold in the absence of TiO_2.

The potential application of the as-prepared CS–TiO_2 macroporous monoliths was evaluated by testing scaffold sections for their activity as photocatalysts for the oxidative degradation of certain organic molecules.[15,24,29–32] When incubated in methylene blue or Orange II solutions, the white CS–TiO_2 scaffolds turned blue or orange in color, respectively, indicating strong adsorption of the dye molecules. Subsequent irradiation with UV light for 20 or 5 h resulted in decolorization of the methylene blue or Orange II-loaded CS–TiO_2 scaffolds, respectively, confirming that the scaffold sections exhibited substantial photocatalytic activity. The faster rate of photodegradation of the Orange II molecules was attributed to increased adsorption of the anionic dye on the surface of the positively charged chitosan matrix compared with surface binding of cationic methylene blue. In contrast, no decolorization of the dye solutions was observed for cross-linked CS scaffolds prepared in the absence of TiO_2 particles. Time-dependent log concentration plots ($\ln(C_0/C)$ *vs.* t) confirmed that the kinetics of photodegradation followed first order behavior in good agreement with a Langmuir–Hinshelwood mechanism (Fig. 6a and b).[31,32] The apparent first order rate constants for methylene blue were 0.033, 0.161 or 0.162 min^{-1} for scaffolds prepared with anatase nanoparticles, K-TiO_2 or P-25 TiO_2, respectively. Analogous values for Orange II photodegradation were 0.385, 0.250 and 0.221 min^{-1}, respectively.

The results indicated that the rate of methylene blue degradation for P-25 and K-TiO_2-loaded scaffolds was significantly higher than that measured for monoliths prepared with 6 nm sized anatase particles (Fig. 6a). This was attributed to the increased accessibility of the larger P-25 and K-TiO_2 particles, which unlike the anatase nanoparticles remained exposed on the internal walls of the scaffolds (see Fig. 4). In contrast, the catalytic degradation profiles for Orange II showed similar reaction kinetics for each of three types of TiO_2 colloids (Fig. 6b), presumably because electrostatic interactions between the positively charged (acid-peptized) 6 nm sized TiO_2 nanoparticles and anionic Orange II dye molecules were sufficient to offset the relatively low surface accessibility of this colloid. The above observations were consistent with control experiments on the catalytic activities of colloidal dispersions of TiO_2 nanoparticles in the absence of chitosan, which indicated that the efficiencies in methylene blue degradation associated with 6 nm sized anatase or P-25 particles were higher than for K-TiO_2 (ESI,† Fig. S6). Similarly, the trend in degradation efficiency for Orange II was 6 nm anatase > P-25 > K-TiO_2.

In order to determine the potential reusability of the composite scaffolds, a second cycle of photocatalysis was tested without performing any cleaning process. Comparison of the photocatalytic activities indicated that methylene blue photodegradation was maintained using the P-25 and K-TiO_2 doped macroporous monoliths, whereas the activity was reduced by ~10% on the second cycle with a scaffold prepared with the anatase nanoparticle sol (Fig. 6c). In contrast, the latter showed unchanged activity whilst K-TiO_2 and P-25 scaffolds exhibited minimal decrease in the photocatalytic degradation of Orange II (Fig. 6d).

Conclusions

3D-Macroporous cross-linked CS–TiO_2 scaffolds with photocatalytic properties were successfully prepared *via* ice-templating processing. The internal morphology and microstructure of the composite monoliths were controlled and optimized by varying parameters such as solute concentrations and freezing rate. SEM studies revealed that the TiO_2 particle size had a significant effect on the micro-channeled structure. Homogenous mixtures of a TiO_2 (anatase) sol and GPTMS-cross-linked chitosan gel produced monoliths with smooth interior walls due to

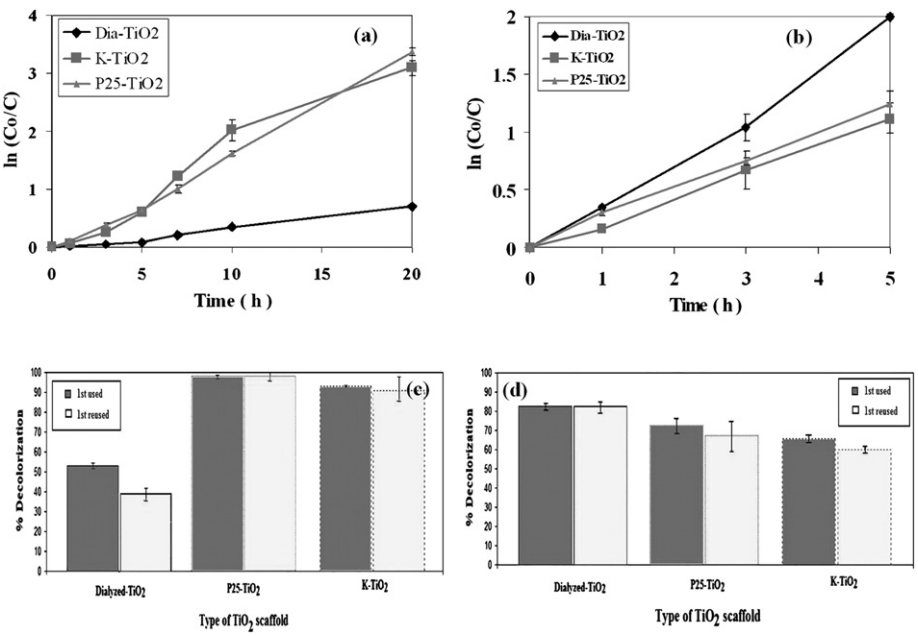

Fig. 6 Photocatalytic degradation plots showing % decolorization for (a) methylene blue and (b) Orange II adsorbed onto various macroporous CS–TiO_2 scaffolds. (c,d) Photocatalytic reusability of macroporous CS–TiO_2 scaffolds with adsorbed methylene blue (c) or Orange II (d). Two photodegradation cycles were performed for each scaffold and the change in absorbance of the dye solution was recorded at 1 h time interval.

incorporation of the nanoparticles within the polysaccharide matrix. On the other hand, P-25-TiO_2 and K-TiO_2 particles were only partially embedded in the chitosan scaffold, such that these particles were often exposed at the surface of the channel walls. As a result, the mechanical properties and photocatalytic activity of the monoliths were influenced by their associated microstructure. In particular, the mechanical strength was in the order of TiO_2 nanoparticles > K-TiO_2 > P-25, and although all the CS–TiO_2 scaffolds displayed photocatalytic activity, monoliths containing anatase nanoparticles were less active in methylene blue degradation. Moreover, the hybrid scaffolds were reusable and retained their degradation efficiency on a second photocatalytic cycle. These observations clearly suggest that ice-templating routes offer a simple fabrication method to the construction of a wide range of functional 3D membrane reactors where desired electronic, catalytic, biosensing and mechanical properties can be simply tuned by appropriate choice of the constituent phases.

Acknowledgements

This research was supported by the Thailand Research Fund through the Royal Golden Jubilee Ph.D. Program (Grant No. PHD/0197/2548), the Graduate School-PSU through the Thesis Research Fund, and partially supported by the Center of Innovation in Chemistry: Postgraduate Education and Research Program in Chemistry (PERCH-CIC) to C.S.

References

1 G. J. D. Solerillia, C. Sanchez, B. Lebeau and J. Patarin, *Chem. Rev.*, 2002, **102**, 4093.
2 S. W. Boettcher, J. Fan, C.-K. Tsung, Q. Shi and G. D. Stucky, *Acc. Chem. Res.*, 2007, **40**, 784.
3 F. Laeri, F. Schuth, U. Simon and M. Wark, *Host–Guest Systems Based on Nanoporous Crystals*, Wiley-VCh, Verlag GmbH & Co., Weinheim, 2003.
4 G. Q. Lu and X. S. Zhao, *Nanoporous Materials-Science and Engineering, Series on Chemical Engineering*, Imperial College Press, UK, 2004, vol. 4.
5 H. Nishihara, S. R. Mukai, D. Yamashita and H. Tamon, *Chem. Mater.*, 2005, **17**, 683.
6 K. Whang, C. H. Thomas and K. E. Healy, *Polymer*, 1995, **36**, 837.
7 Y. S. Nam, J. J. Yoon and T. G. Park, *J. Biomed. Mater. Res.*, 2000, **53**, 1.
8 A. G. Mikos, G. Sarakinos, S. M. Leite, J. P. Vacanti and R. Langer, *Biomaterials*, 1993, **12**, 323.
9 Q. L. Zhou, Y. H. Gong and C. Y. Gao, *J. Appl. Polym. Sci.*, 2005, **98**, 1373.
10 R. Nazarov, H.-J. Jin and D. L. Kaplan, *Biomacromolecules*, 2004, **5**, 718.
11 B. Zhang, S. A. Davis and S. Mann, *Chem. Mater.*, 2002, **14**, 1369.
12 M. C. Gutierrez, M. L. Ferrer and F. del Monte, *Chem. Mater.*, 2008, **20**, 634.
13 A. I. Cooper, *Adv. Mater.*, 2003, **15**, 1049.
14 H. Nishihara, S. R. Mukai, Y. Fujii, T. Tago, T. Masuda and H. Tamon, *J. Mater. Chem.*, 2006, **16**, 3231.
15 M. Nieto-Suarez, G. Palmisano, M. L. Ferrer, M. C. Gutierrez, S. Yurdakal, V. Augugliaro, M. Pagliaro and F. del Monte, *J. Mater. Chem.*, 2009, **19**, 2070.
16 S. R. Mukai, H. Nishihara, S. Shichi and H. Tamon, *Chem. Mater.*, 2004, **16**, 4987.
17 S. Deville, E. Saiz and A. P. Tomsia, *Acta Mater.*, 2007, **55**, 1965.
18 M. C. Gutierrez, M. Jobbagy, M. L. Ferrer and F. del Monte, *Chem. Mater.*, 2008, **20**, 11.
19 H. Zhang, I. Hussain, M. Brust, M. F. Butler, S. P. Rannard and A. I. Cooper, *Nat. Mater.*, 2005, **4**, 787.
20 M. C. Gutierrez, Z. Y. Garcia-Carvajal, M. Jobbagy, F. Rubio, L. Yuste, F. Rojo, M. Jobbagy, M. L. Ferrer and F. del Monte, *Adv. Funct. Mater.*, 2007, **17**, 3505.
21 M. C. Guiterrez, M. J. Hortiguela, J. M. Amarilla, R. Jimenez, M. L. Ferrer and F. del Monte, *J. Phys. Chem. C*, 2007, **111**, 5557.
22 M. C. Guiterrez, Z. Y. Garcia-Carvajal, M. J. Hortiguela, L. Yuste, F. Rojo, M. L. Ferrer and F. del Monte, *J. Mater. Chem.*, 2007, **17**, 2992.
23 J. L. Vickery, A. J. Patil and S. Mann, *Adv. Mater.*, 2009, **21**, 2180.
24 M. R. Hoffmann, S. T. Martin, W. Choi and D. W. Bahnemann, *Chem. Rev.*, 1995, **95**, 69.
25 G. Oskam, A. Nellore, R. Lee Penn and P. C. Searson, *J. Phys. Chem. B*, 2003, **107**, 1734.
26 C. Suwanchawalit and S. Wongnawa, *Appl. Catal., A*, 2008, **338**, 87.
27 Y. L. Liu, Y. H. Su and J. Y. Lai, *Polymer*, 2004, **45**, 6831.
28 Y. Zhang and A. Weidenkaff, *Mater. Lett.*, 2002, **54**, 375.
29 J. Bandara, J. A. Mielczarski and J. Kiwi, *Langmuir*, 1999, **15**, 7680.
30 K. Tanaka, K. Padermpole and T. Hisanaga, *Water Res.*, 2000, **34**, 327.
31 A. Houas, H. Lachhebm, M. Ksibi, E. Elaloui, C. Guillard and J.-M. Herrrmann, *Appl. Catal., B*, 2001, **31**, 145.
32 A. B. Prevot, C. Baiocchi, M. C. Brussino, E. Pramauro, P. Savarino, V. Augugliaro, C. Marc and L. Palmisano, *Environ. Sci. Technol.*, 2001, **35**, 971.